A novel inflammation-associated prognostic signature for clear cell renal cell carcinoma

GANGCHENG LIU[1*], DONGLAN XIONG[2*], ZHIFEI CHE[3*], HUALEI CHEN[4] and WENYI JIN[5]

Departments of [1]Urology Surgery and [2]Respiratory Medicine, Affiliated Renhe Hospital of China Three Gorges University Second Clinical Medical College of China Three Gorges University, Yichang, Hubei 443000; [3]Department of Urology, The First Affiliated Hospital of Hainan Medical University; [4]Department of Urology Surgery, The Second Affiliated Hospital of Hainan Medical University, Haikou, Hainan 570100; [5]Department of Orthopedics, Renmin Hospital of Wuhan University, Wuhan, Hubei 430060, P.R. China

Received February 1, 2022; Accepted May 20, 2022

DOI: 10.3892/ol.2022.13427

Abstract. Clear cell renal cell carcinoma (ccRCC) are typically situated in a complex inflammatory and immune microenvironment, which has been reported to contribute to the unfavorable prognosis of patients with ccRCC. There would be beneficial clinical implications for elucidating the roles of its molecular characteristics in the inflammatory microenvironment. This is because it would facilitate the development of reliable biomarkers for pre-stratification prior to the designation of individualized treatment strategies. In the present study, RNA-sequencing data from 607 patients were retrospectively analyzed to elucidate the profile of inflammatory molecules. Based on this, an inflammatory prognostic signature (IPS) was developed and further validated using clinical ccRCC samples. Subsequently, the associated mechanisms in terms of the immune microenvironment and molecular pathways were then investigated. This proposed IPS was found to exhibit superior accuracy compared with the criterion of a good prognostic model for the prediction of patient prognosis from ccRCC [area under the receiver operating characteristic curve (AUC)=0.811] in addition to being an independent factor for prognostic risk stratification [hazard ratio: 11.73 (95% CI, 26.98-5.10); log-rank test, P<0.001]. Pathologically, ccRCC cells identified as high-risk according to their IPS presented with a more malignant tumor structure, including voluminous eosinophilic cytoplasm, acinar/lamellar/tubular growth patterns and atypic nuclei. High-risk ccRCC also exhibited higher infiltration levels by four types of immune cells, including T regulatory cells, but lower infiltration levels by mast cells. Pathways associated with immune-inflammation interaction, including the IL-17 pathway, were found to be upregulated in IPS-identified high-risk ccRCC. Furthermore, by combining the IPS with clinical factors, an integrated prognostic index was developed and validated for increasing the accuracy of patient risk-stratification for ccRCC (AUC=0.911). In conclusion, the complex regulatory mechanisms and molecular characteristics involved in ccRCC-inflammation interaction, coupled with their prognostic potential, were systematically elucidated in the present study. This may have important implications in furthering the understanding into the molecular mechanisms underlying this ccRCC-inflammation interaction, which can in turn be exploited for identifying high-risk patients with ccRCC prior to designing their clinical treatment strategy.

Correspondence to: Dr Wenyi Jin, Department of Orthopedics, Renmin Hospital of Wuhan University, 238 Zhangzhidong Road, Wuchang, Wuhan, Hubei 430060, P.R. China
E-mail: gin1994@whu.edu.cn

Dr Hualei Chen, Department of Urology Surgery, The Second Affiliated Hospital of Hainan Medical University, 368 Yehai Road, Haikou, Hainan 570100, P.R. China
E-mail: dochualei@sina.com

*Contributed equally

Abbreviations: ccRCC, clear cell renal cell carcinoma; IPS, inflammation-associated prognostic signature; FPKM, fragments per kilobase of exon model per million mapped fragments; IGs, inflammation-associated genes; LASSO, least absolute shrinkage and selection operator; AIC, Akaike information criterion; ROC, receiver operating characteristic; AUC, area under ROC curve; KEGG, Kyoto Encyclopedia of Genes and Genomes; PPI, protein-protein interaction; CIBERSORT, cell type identification through the estimation of relative subsets of RNA transcripts; IGPs, IGs that impact the prognosis of patients with ccRCC; Tregs, T regulatory cells; IPI, integrated prognostic index

Key words: clear cell renal cell carcinoma, inflammation, immune cells, prognostic signature, precision medicine

Introduction

As the most prevalent type solid renal tumors, the prevalence of renal cell carcinoma (RCC) has been increasing with a prevalence of 2-4% over recent decades (1). Among other subtypes of renal cancers, clear cell renal cell carcinoma (ccRCC) has become of increasing concern due to its high rate of occurrence (>90% of all RCC cases) and declining overall survival rate (2,3). Effective adjuvant therapy remains an urgent unfulfilled requirement for reducing the risk of

recurrence whilst improving outcomes. Previous studies have explored the possibility of chemotherapy, radiotherapy, cytokine therapy, hormonal treatment therapy and tumor cell vaccines as potential adjuvant options (4,5). However, all of these studies yielded disappointing results (4,5). Therefore, tailored treatment strategies are becoming increasingly reliant on accurate risk-stratification approaches (6-8), which offer hope to patients with ccRCC for improving the curative effects of implemented interventions and the long-term survival rate.

For making clinical intervention decisions, recent risk-stratification characteristics remain insufficient, since and 20-30% patients who were diagnosed with T1-2 stages ccRCC suffered from metastasis within 1-2 years following surgery (6,9). Emerging biomarkers have been previously proposed based on multi-gene signatures or clinical features (7-9). However, due to the technological bias across the high-throughput platforms and difference among normalization methods, their predictive ability remains limited and will scarcely be used for the individualized therapy of patients with ccRCC in the foreseeable future (6-8). Therefore, novel biomarkers with higher prognostic predictive potential are urgently required for optimizing the tailored clinical management protocol for patients with ccRCC to achieve significant tumor remission.

Biomarkers based on inflammatory responses or signaling pathways are showing promise for survival estimation and for guiding the design of personalized treatment for patients with ccRCC (10-12). This is mainly due to the impact of inflammation on tumor phenotype and efficacy of clinical treatment (10-12). Inflammation has emerged as one of the main hallmarks of cancer progression (13,14) and has been reported to serve a key role in tumor occurrence and outcome (15,16). Tumor-associated macrophages have been indicated to be stimulators of tumor cell proliferation and facilitators of angiogenesis, invasion and metastasis (17,18). A previous study has shown that inflammatory cytokines and chemokines generated by tumor cells and/or tumor-associated white blood cells and platelets may directly lead to malignant progression in human cancer, including cervix, and head and neck cancers (19). For ccRCC, IL-6 is an inflammatory cytokine with multiple biological effects that has been reported to enhance the proliferation of ccRCC cells (20,21). These reports support the application of anti-inflammatory therapeutics or agents for ccRCC, which have generally demonstrated satisfactory efficacy (10). Simvastatin, which is an inhibitor of the AKT, mTOR and ERK signaling pathways in addition to being an inhibitor of IL-6-induced JAK2/STAT3 activation, was shown to be able to inhibit the proliferation and migration of ccRCC cells (10,22). However, knowledge gaps remain in the field of clinical management regarding the ability of an inflammation-specific prognostic signature to predict the long-term survival rate of patients with ccRCC.

In the present study, the prognostic potential of inflammation-associated molecules in ccRCC was systematically assessed, based on which an inflammation-associated prognostic signature (IPS) was developed using a multi-step process. The IPS was confirmed as being a highly effective and robust biomarker for the prognostic prediction and risk stratification of patients with ccRCC. Of note, the underlying immune mechanisms, dysregulated biological functions and pathways within the interactive network of identified inflammation-associated genes (IGs) were clarified to understand the processes that can impact the overall survival time in the low- and high-risk groups. To facilitate clinical application, a nomogram combining IPS and clinical characteristics was developed.

Materials and methods

Data retrieval and processing. RNA expression data obtained by RNA sequencing and the clinical records of 607 patients with ccRCC were acquired from The Cancer Genome Atlas (www.tcga.org). Only patients with complete clinical records were included in the study, which resulted in the study's sample size being reduced to 522.

In addition, six clinical samples of ccRCC (mean ± SD age, 51±13.48 years; 5 males and, 1 female) were collected from patients at the Renmin Hospital of Wuhan University (Wuhan, China) between March 2017 and May 2018. Inclusion criteria: Only ccRCC was included. Low-grade ccRCC: No lymph node metastasis and distant metastasis. High-grade ccRCC: Lymph node metastasis or distant metastasis occurred. Exclusion criteria: Exclusion papillary carcinoma and chromophobe renal carcinoma. Low-grade ccRCC: Lymph node metastasis and distant metastasis occurred. High-grade ccRCC: No lymph node metastasis or distant metastasis. Full informed consent in written form was provided by those subjects and the Ethics Committee of Renmin Hospital of Wuhan University issued the ethical approval (approval no. 2017K-C015). The clinicopathological data of these 6 patients are presented at Table SI.

RNA expression data were standardized using fragments per kilobase of exon model per million mapped fragments (FPKM) and then converted using the following formula to facilitate further analysis: Gene expression=$\log_2$(FPKM +1).

Public data for the present study were acquired in October 2020 and analyzed between November and December 2020. For further prognostic signature modeling and validation, the overall study cohort was randomly divided 1:1 into the training cohort and validation cohort.

Identification of IGs impacting the prognosis of patients with ccRCC. According to the dataset provided by the Gene Ontology (GO) database (geneontology.org), genes involved in inflammatory responses and pathways considered to be IGs were retrieved by filtering terms containing 'inflammatory' or 'inflammation' (Table SII). The IG expression profiles were extracted from the converted RNA expression profiles of patients with ccRCC. Iterative univariate Cox regression and log-rank tests were then performed via R software (version 4.0.2) for each extracted IG of a clinical sample of ccRCC. IGs with $P<0.05$ from both Cox regression and log-rank tests were considered to be those that significantly impacted the prognosis of patients with ccRCC (IGPs). In the present study, prognosis is represented by overall survival (OS).

IPS modeling. To minimize the risk of overfitting, least absolute shrinkage and selection operator (LASSO) regression was used to create subsets of candidate IGPs. LASSO regression was performed using the 'glmnet' package (version 4.0) in

R (23). Upon completion, multicollinear IGPs and IGPs that had little influence on ccRCC prognosis were eliminated using the stepwise method (24). With this typical method, the Akaike information criterion (AIC) approach (24) was used for eliminating independent variables that share little association with the dependent variable. The model with the smallest AIC during the stepwise process was considered to be the best model. Therefore, the IPS was constructed using a multivariate Cox proportional-hazards regression model, which was calculated using the following formula (24):

$$\text{IPS score} = \sum_{i=1}^{n} \beta_i x E_i$$

Where n represents the total number of IGPs included in the IPS, β_i represents the regression coefficient of gene i and E_i represents the converted expression level of gene i. For the present study, the 'survival' package (25) in R software was used for constructing the IPS.

Validation of the IPS. A receiver operating characteristic (ROC) curve was used to calculate the area under the ROC curve (AUC), which was then applied to evaluate the accuracy of prognosis prediction by IPS. As previously reported (26), an optimal cut-off value of the IPS score was derived using the Youden index in the ROC curve from the training cohort for classifying patients with ccRCC into the high- or low-risk groups. Kaplan-Meier curve and log-rank test were then used to detect any potential difference between the high- and low-risk groups in the training and validation cohort. To validate whether the IPS is able to independently predict the prognosis of patients with ccRCC, univariate and multivariate Cox regression analyses were performed in the training and validation cohort. For further investigation of the correlation between the IPS score and overall survival time of patients with ccRCC, Pearson's correlation analysis was performed. The Kaplan-Meier, log-rank, ROC curve and Cox regression were all performed using the 'rms', 'survival' and 'survminer' packages in R software, where the results of each were visualized in R software.

Functional annotation and analysis. For clarifying the biological roles of the IGPs in the development of ccRCC, GO and Kyoto Encyclopedia of Genes and Genomes (KEGG) enrichment analyses were performed in R software to elucidate the biological processes, cellular components, molecular functions and pathways regulated by the IGPs; an adjusted P-value of <0.05 was deemed as statistically significant. To further determine the interactive networks among the IGPs, a protein-protein interaction (PPI) network analysis was performed using the STRING dataset (string-db.org; version 11.5, interaction score >0.4) and visualized using Cytoscape software (version 3.0.1).

Differences in immune cell infiltration between risk groups. Cell type identification through the estimation of relative subsets of RNA transcripts (CIBERSORT) is a deconvolution algorithm that was developed by Newman *et al* (27). It was used for the calculation of the abundance of infiltrating immune cells for each sample included in the study, based on 22 sets of data containing the profiles of infiltrating immune cell-associated genes (27). The degree of immune cell infiltration in the low- and high-risk groups was estimated using CIBERSORT and its provided gene set LM22 (27). According to a previous study (24), the CIBERSORT algorithm was applied with 1,000 simulations and the results were filtered with P<0.05.

Reverse transcription-quantitative PCR (RT-qPCR). In line with the protocol of a previous study (28), reverse transcription and qPCR were performed according to the instructions provided by the manufacturer [PrimeScript™ RT reagent kit with gDNA Eraser; cat no. RR047A; TB Green Premix Ex Taq II (Tli RNase H Plus); cat. no. RR820A; both from Takara Bio, Inc.]. In brief, total RNAs were purified from six clinical ccRCC samples using TRIzol® agent (cat. no. R0016; Beyotime Institute of Biotechnology), and then the purified RNAs were incubated with gDNA Eraser for 2 min at 42˚C to erase gDNA and then transcribed into cDNA by using the PrimeScript™ RT Enzyme Mix I and RT Primer Mix (37˚C for 15 min and then 85˚C for 5 sec). Subsequently, real-time fluorescent qPCR was used to measure the relative corresponding gene expression relative to GAPDH using the following conditions: 40 cycles of 95˚C for 5 sec and 60˚C for 35 sec. Quantification was performed using the $2^{-\Delta\Delta Cq}$ method (29). The primers were as follows (30-41): ADCY1 forward, 5'-CAGCACTTCCTCATGTCCAA-3' and reverse, 5'-CCAGTGCTATCCATCCGACT-3'; ADIPOQ forward, 5'-TGGTGAGAAGGGTGAGAA-3' and reverse, 5'-AGATCT TGGTAAAGCGAATG-3'; ADORA2B forward, 5'-TGC ACTGACTTCTACGGCTG-3' and reverse, 5'-GGTCCCCGT GACCAAACTT-3'; CCL7 forward, 5'-GCCTCTGCAGCA CTTCTGTG-3' and reverse, 5'-CACTTCTGTGTGGGGTCA GC-3'; CXCL3 forward, 5'-GCAGGGAATTCACCTCAA GA-3' and reverse, 5'-GGTGCTCCCCTTGTTCAGTA-3'; GPS2 forward, 5'-AGTGACCTGACCACCCTAACA-3' and reverse, 5'-CCTGGGCGATTGTGTCCTC-3'; HGF forward, 5'-TGGGACAAGAACATGGAAGA-3' and reverse, 5'-GCA TCATCATCTGGATTTCG-3'; IL1RL2 forward, 5'-TCTTAT ACCCCAAGTACCCG-3' and reverse, 5'-ACTGCTCTGTGA AGTCCCC-3'; IL4 forward, 5'-TCTCACCTCCCAACTGCT TCCCC-3' and reverse, 5'-AGAGGTTCCTGTCGAGCCGTT TCA-3'; IL17C forward, 5'-CAACCGATCCACCTCACC TT-3' and reverse, 5'-GGCACTTTGCCTCCCAGAT-3'; IL22 forward, 5'-CACTGCAGGCTTGACAAG-3' and reverse, 5'-CTTAGCCTGTTGCTGAGC-3'; LIPA forward, 5'-TCT GGACCCTGCATTCTGAG-3' and reverse, 5'-CACTAGGGA ATCCCCAGTAAGAG-3'; LRRC19 forward, 5'-ATGAAA GTCACAGGCATCACAATCC-3' and reverse, 5'-'ATTTTC TTCACATAATTCATGGATA-3'; LTB4R2 forward, 5'-GGG TGTAAAGGGACGTGCACAG-3' and reverse, 5'-GCTTGT GCTGTTTCCTGGCAAG-3'; RORA forward, 5'-AAAAAC ATGGAGTCAGCTCCG-3' and reverse, 5'-AGTGTTGGC AGCGGTTTCTA-3'; SOCS3 forward, 5'-ACAATCTGCCTC AATCACTCTG-3' and reverse, 5'-TTGACTTGGATTGGGA TTTTG-3'; TPSB2 forward, 5'-GTGAAGGTCCCCATAATG GAAAA-3' and reverse, 5'-CACAGCATGTCGTCACGGA-3'; WNT5A forward, 5'-CGCCCAGGTTGTAATTGAAG-3' and reverse, 5'-GCATGTGGTCCTGATACAAGT-3'; and GAPDH forward, 5'-GGTGAAGGTCGGAGTCAACG-3' and reverse, 5'-TGGGTGGAATCATATTGGAACA-3'.

H&E staining and immunohistochemistry (IHC). H&E staining and IHC were performed according to a previous study (1). The renal cancer tissue was fixed with 4% paraformaldehyde, embedded in paraffin, and cut into slices (3-μm thick per specimen). The slices were baked at 60˚C for 1 h, followed by deparaffinizing; the slices were placed in xylene 3 times for 10 min each and wash with ethanol gradient for 5 min. Slices were then stained with hematoxylin for 10 min at 25˚C, and rinsed back to blue, before staining with eosin for 5 min at 25˚C, and then rehydrating (rinse and dehydrate with gradient alcohol 3 times for 3 min each, and place in xylene 3 times for 5 min each). Finally, the slides were sealed with neutral gum, and observed and imaged under an orthophoto microscope (BX63; Olympus Corporation). For IHC, the sections were deparaffinized, hydrated, subjected to heat for antigen retrieval in 10 mM sodium citrate (pH, 6.0) for 15 min at 95˚C and treated with 3% hydrogen peroxide for 10 min to inactivate the endogenous peroxidase. After blocking with 5% goat serum (Beyotime Institute of Biotechnology) for 30 min at 25˚C, the sections were incubated overnight with primary antibodies against IL22 (1:100; cat. no. ab227033; Abcam), IL4 (1:400; cat. no. ab62351; Abcam), CCL7 (1:200; cat. no. ab228979; Abcam) and LTB4R2 (1:200; cat. no. ab84600; Abcam) at 4˚C. The sections were then incubated with horseradish peroxidase-conjugated secondary antibody (1:200; cat. no. GB23303; Wuhan Servicebio Technology Co., Ltd.) for 1 h at 25˚C, washed with PBS for 10 min and stained with diaminobenzidine (cat. no. A600140; Sangon Biotech, Co., Ltd.). Images were obtained under an orthophoto microscope (BX63; Olympus Corporation). Next, R software (version 4.0.2) was used for visualization. The total and positively stained cells of the tissue sections were counted at x200 magnification (scale bar, 50 μm), and the percentage of positive cells was calculated using ImageJ software (version 1.8.0).

Statistical analysis. R software (version 4.0.2; www.R-project.org/) was used for bioinformatics and statistical analyses. For experimental validation, ≥ three biological repetitions were performed. To perform grouped comparisons, Kruskal-Wallis test (H-test, a pairwise comparison using Dwass-Steel-Critchlow-Fligner test and P-value adjustment using the Benjamini and Hochberg method) was applied using the 'ggstatplot' package in R (42).

Results

Construction and definition of the IPS. A total of 522 cases of ccRCC were included in the present study. Their demographic data and clinical characteristics are provided in Table I, including age (210 patients >61 years and 312 patients ≤61 years) and sex (369 males and 153 females). Regarding the list of genes associated with the inflammatory responses and pathways that were provided by the GO dataset, the expression profiles of 626 IGs were extracted from the 56,753 genes analyzed in each sample. Feature selection and IPS modeling were then performed for the training cohort. IGPs were detected using iterative univariate Cox regression and the log-rank test. As presented in Table SIII, a total of 43 IGPs were detected and used for further IPS modeling. In order to minimize the risk of overfitting, LASSO regression was performed, as well as the gene selection process, optimal λ calculation and coefficient changes (Fig. 1A and B). After screening, 36 IGPs remained for final IPS modeling. Cox proportional hazards model was trained using the AIC-based stepwise method to generate IPS, which contained 18 IGPs (Table II).

Table I. Demographic characteristics of the included patients.

Parameter	Patients, n
Age, years	
>61	210
≤61	312
Sex	
Male	369
Female	153
Neoplasm histological grade	
G1	11
G2	188
G3	179
G4	144
Pathologic T-stage	
T1	19
T1a	115
T1b	95
T2	46
T2a	10
T2b	2
T3	4
T3a	105
T3b	43
T3c	1
T4	82
Pathological N-stage	
N0	208
N1	314
Pathological M-stage	
M0	335
M1	187

Validation of IPS as an independent prognostic factor. For the classification of patients with ccRCC, ROC curve analysis was used to derive an optimal cut-off value for the IPS score, which was 1.14 in the training cohort. Based on this, patients with an IPS score >1.14 were classified as members of the high-risk group, whilst others were classified as low-risk group members (Fig. 2A). The distribution of IPS scores and outcomes for each patient in the different risk groups in the training cohort are presented in Fig. 2A. It was observed that the overall survival time of patients in the high-risk group was shorter compared with that of patients in the low-risk group (Fig. 2A). In addition, the number of events (deaths) in the high-risk group was higher compared with that in the low-risk group (Fig. 2A). Similar trends could also be observed in the validation cohort (Fig. 2B). The differential expression profiles

Table II. Coefficients of genes included in the inflammatory prognostic signature.

Genes	Coefficient	Hazard ratio	95% CI	P-value
ADCY1	-0.551	0.576	0.364-0.911	0.018408
ADIPOQ	0.353	1.424	1.033-1.962	0.031072
ADORA2B	0.323	1.381	0.995-1.917	0.053474
CCL7	0.993	2.699	1.772-4.112	$3.80x10^{-6}$
CXCL3	-0.657	0.518	0.361-0.744	0.000368
GPS2	0.335	1.399	0.925-2.115	0.112054
HGF	0.171	1.186	1.020-1.379	0.026637
IL1RL2	-0.355	0.701	0.513-0.958	0.025736
IL4	3.465	31.968	5.549-184.154	0.000105
IL17C	-5.383	0.005	0.000-0.072	0.000126
IL22	8.456	4705.498	33.107-668798.685	0.000826
LIPA	-0.266	0.767	0.601-0.977	0.031965
LRRC19	-0.170	0.844	0.708-1.005	0.057198
LTB4R2	0.463	1.589	0.917-2.753	0.098503
RORA	-0.585	0.557	0.347-0.894	0.015301
SOCS3	0.257	1.293	1.105-1.513	0.001324
TPSB2	-0.306	0.736	0.626-0.866	0.000217
WNT5A	0.282	1.326	0.968-1.817	0.079332

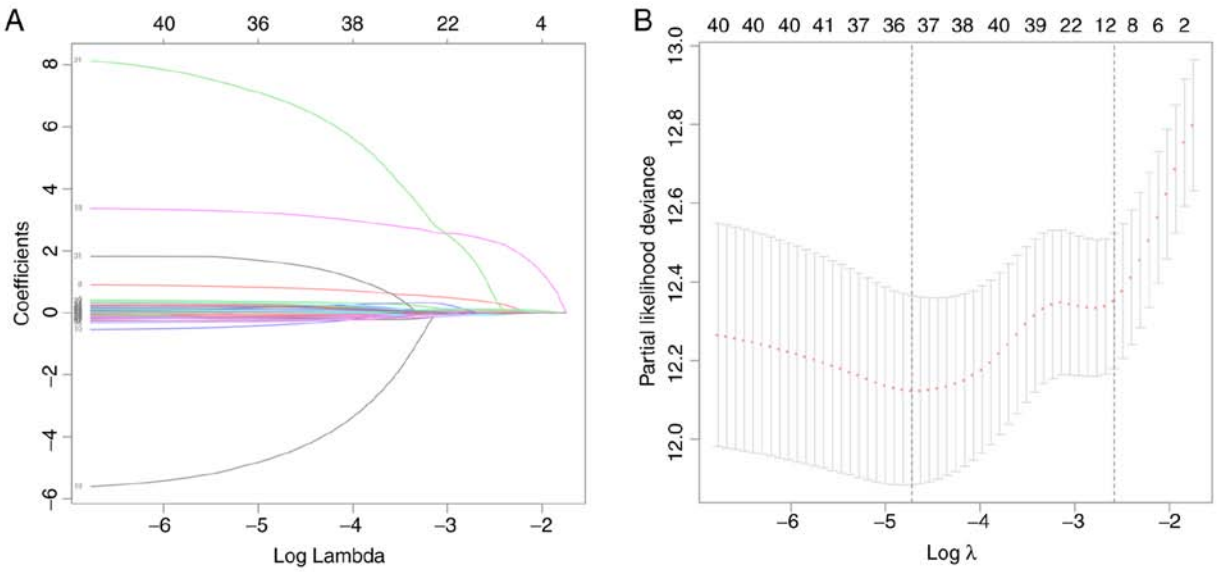

Figure 1. Results of feature selection using least absolute shrinkage and selection operator regression. (A) Coefficients and (B) partial likelihood deviance. The number of genes are presented at the top of each panel.

of IGPs constituting the IPS in the low- and high-risk groups are provided in Fig. 2C. For evaluating the prediction accuracy of the IPS, ROC curves and their AUC were calculated in the training and validation cohort. As presented in Fig. 2D, regarding the reported judgment criteria (AUC >0.7) for the predictive ability of the prognostic model (43), IPS achieved high accuracy for the prediction of the prognosis of patients with ccRCC (AUC=0.811 in the training cohort). A similar trend in AUC was also observed in the validation cohort (AUC=0.799), suggesting further that this IPS is robust. Kaplan-Meier curve analysis with the log-rank test was subsequently applied for detecting the difference in overall survival probability between the low- and high-risk groups. As indicated by the results in Fig. 2E, high-risk patients with ccRCC had a significantly lower overall survival probability compared with that in patients in the low-risk group in the training cohort (P<0.001). Similar results were found in the validation cohort (Fig. 2F). In terms of progression-free survival (PFS), high-risk patients according to IPS also demonstrated a lower probability of PFS in the training (Fig. S1) and validation cohorts (Fig. S2). The resultant data demonstrated the viability of this developed IPS for the risk-stratification of patients with ccRCC. This IPS

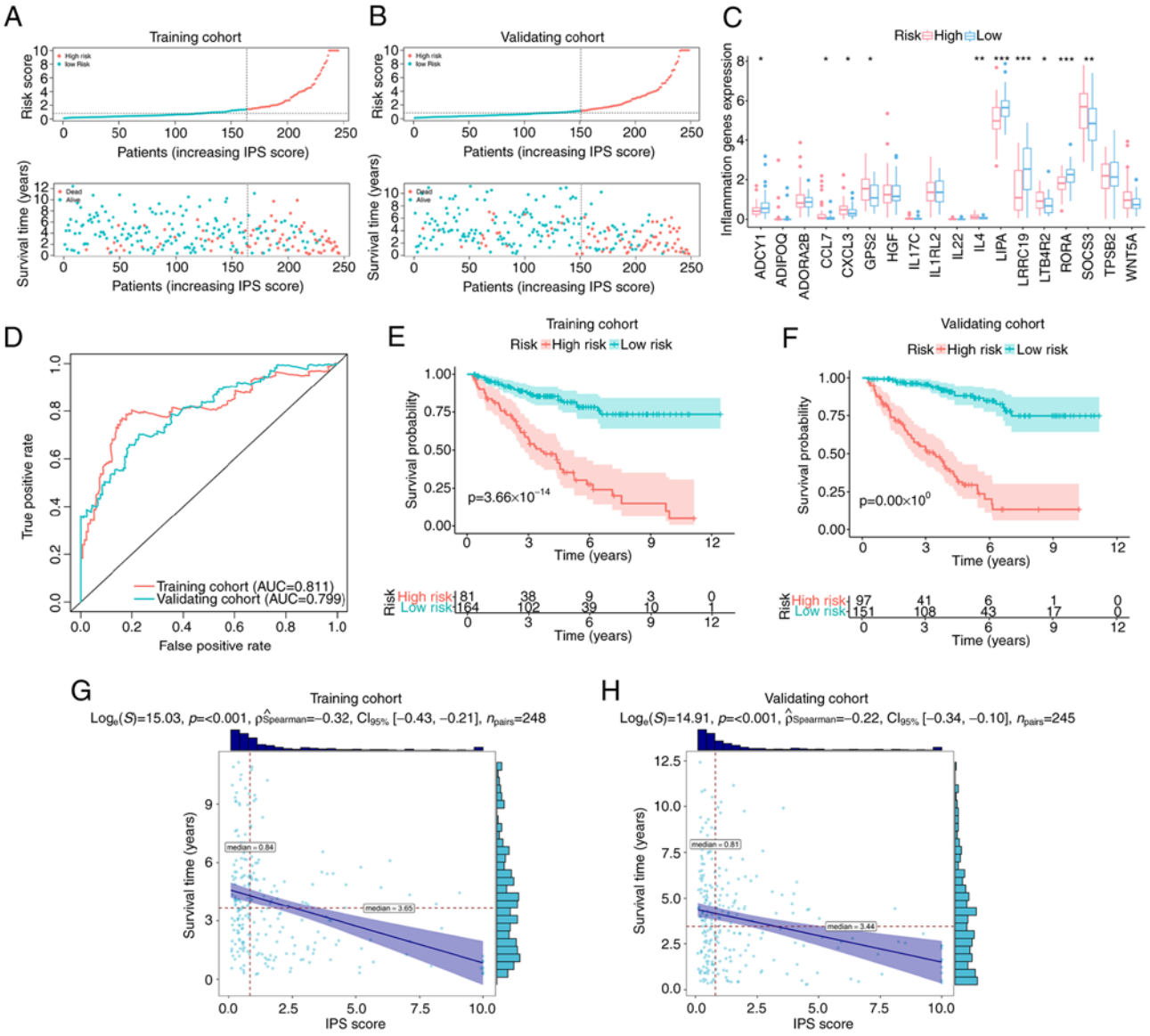

Figure 2. Validation of IPS. Distribution plots for the IPS score, overall survival time and survival status of each patient with clear cell renal cell carcinoma in the (A) training cohort and (B) validation cohort. (C) Differential expression profiles of inflammation-associated genes constituting the IPS between IPS-identified high- and low-risk groups, with dots above indicating outliers. Box plots show the five-number summary of a set of data, including the minimum score, first (lower) quartile, median, third (upper) quartile and maximum score. (D) ROC curves of IPS in the training and validation cohort. Kaplan-Meier curves indicating the difference in survival probability between the IPS-identified high-risk and low-risk groups in (E) the training cohort and (F) validating cohort. Correlation analyses attested the association between the IPS score and survival time in (G) the training cohort and (H) validation cohort. IPS, inflammatory prognostic signature; AUC, area under the ROC curve; ROC, receiver operating characteristic. *P<0.05, **P<0.01 and ***P<0.001.

score exhibited a negative correlation with the overall survival time in both the training cohort (ρ=-0.32, P<0.001; Fig. 2G) and the validation cohort (ρ=-0.22, P<0.001; Fig. 2H). These data suggest that the overall survival time of patients with ccRCC decreased as the IPS score increased.

To assess if this IPS score can serve as an independent prognostic factor, univariate and multivariate Cox regression analyses were performed on the training cohort and validation cohort, respectively. As indicated by the results presented in Table III, the P-values of the IPS scores were <0.001 according to both univariate and multivariate Cox regression in the training and validation cohort. This suggest that the IPS score can be used as an independent prognostic factor for patients with ccRCC. In particular, univariate Cox regression revealed that the risk of unfavorable prognosis (shorter overall survival time or death) in the high-risk group was enhanced by 1,073% in the training cohort [hazard ratio (HR)=11.73; 95% CI, 5.10-26.98; P<0.001]. Additionally, this association remained stable even after other covariates were included (Table III). Similar trends were observed in the validation cohort, where all HRs of the IPS scores were higher compared with those of the clinical characteristics in the corresponding analyses (Table III). These results suggest that the IPS score has high predictive power for the risk of poor outcomes and that it associates more closely with prognosis compared with other common clinical characteristics.

Mechanisms of unfavorable prognosis of high-risk patients with ccRCC. To uncover the roles of these IGPs in the development of ccRCC, GO annotation and KEGG enrichment

Table III. Independent analyses using univariate and multivariate Cox regression.

A, Training cohort

	Univariate		Multivariate	
Variable	HR (95% CI)	P-value	HR (95% CI)	P-value
IPS (cut-off 1.14)	11.735 (5.104-26.981)	$6.72x10^{-9}$	11.690 (4.588-29.788)	$2.57x10^{-7}$
Age, years (cut-off 61)	1.020 (0.993-1.048)	0.147098	1.035 (0.994-1.077)	0.095488
Sex	0.728 (0.386-1.374)	0.327579	1.685 (0.771-3.68)	0.190771
Neoplasm histological grade	2.192 (1.408-3.414)	0.000514	2.006 (1.141-3.529)	0.015643
Pathologic T-stage	6.934 (3.645-13.191)	$3.60x10^{-9}$	7.939 (1.653-38.137)	0.009668
Pathologic N-stage	2.249 (0.795-6.363)	0.126733	2.089 (0.564-7.743)	0.270389
Pathologic M-stage	1.962 (1.333-2.887)	0.000634	0.855 (0.317-2.303)	0.756184
Stage	2.169 (1.565-3.006)	$3.29x10^{-06}$	0.931 (0.331-2.621)	0.892045

B, Validation cohort

	Univariate		Multivariate	
Variable	HR (95% CI)	P-value	HR (95% CI)	P-value
IPS (cut-off 1.14)	4.499 (2.440-8.295)	$1.45x10^{-6}$	4.211 (2.131-8.320)	$3.50x10^{-5}$
Age, years (cut-off 61)	1.017 (0.992-1.043)	0.186949	1.031 (1.003-1.059)	0.027546
Sex	1.582 (0.860-2.911)	0.139997	1.555 (0.801-3.018)	0.191663
Neoplasm histologic grade	1.910 (1.295-2.818)	0.001094	0.986 (0.593-1.637)	0.955512
Pathologic T-stage	2.569 (1.328-4.971)	0.005066	1.38 (0.428-4.452)	0.590357
Pathologic N-stage	3.768 (1.476-9.617)	0.005531	0.964 (0.31-3.000)	0.949146
Pathologic M-Stage	1.699 (1.248-2.315)	0.000769	1.045 (0.543-2.013)	0.894424
Stage	1.602 (1.246-2.060)	0.000238	1.415 (0.714-2.805)	0.320424

IPS, inflammatory prognostic signature; HR, hazard ratio.

analysis were performed to elucidate the associated dysregulated biological functions and pathways. KEGG enrichment revealed the dysregulated pathways of IGPs that can promote ccRCC progression (Fig. 3A). the majority of the significantly dysregulated pathways were involved in the inflammatory response or inflammation-immune interaction, including 'cytokine-cytokine receptor interaction', 'IL-17 signaling pathway' and the 'TNF signaling pathway' (Fig. 3B). To further elucidate the biological functions of these IGPs in the progression of ccRCC, GO annotation was performed. The results of the GO annotation provided a molecular regulatory network from three aspects (Fig. 3A). For instance, in the GO category 'biological process', the IGPs participated in the 'Regulation of inflammatory response', 'Negative regulation of response to external stimulus' and 'Positive regulation of cytokine production'. In the GO category 'Cellular component', the IGPs participated in pathways relating to 'The collagen-containing extracellular matrix', the 'Extracellular matrix' and the 'Schaffer collateral-CA1 synapse'. Furthermore, in the GO category 'Molecular function', the IGPs participated in 'Receptor ligand activity', 'Receptor regulator activity' and 'Cytokine activity'. To further detect the interactive network of IGPs constructing IPS, PPI analysis was performed. As presented in Fig. 3C, an interactive network was generated and analyzed, where IL4 was confirmed as the molecule with the most interactions with other IGPs among other IGPs.

Difference in the immune microenvironment between the risk groups. Since the immune microenvironment and inflammation-immunity interactions serve important roles in the development of ccRCC (44,45), differences in the immune microenvironment between the two risk groups were next investigated. CIBERSORT algorithm revealed the immune cell infiltration profiles of each ccRCC clinical sample in the training (Fig. 4A) and validation cohort (Fig. 4B). A total of six immune cell types exhibited significant differences in their infiltration profiles between the low- and high-risk groups. Infiltration by M_0 macrophages, CD4 memory-activated T cells, follicular helper T cells and T regulatory cells (Tregs) were significantly increased in the high-risk ccRCC groups in both the training (Fig. 5A and B) and validation cohorts (Fig. 5C and D). By contrast, infiltration by M_2 macrophages and resting mast cells were significantly decreased in the high-risk ccRCC group in both the training and validation

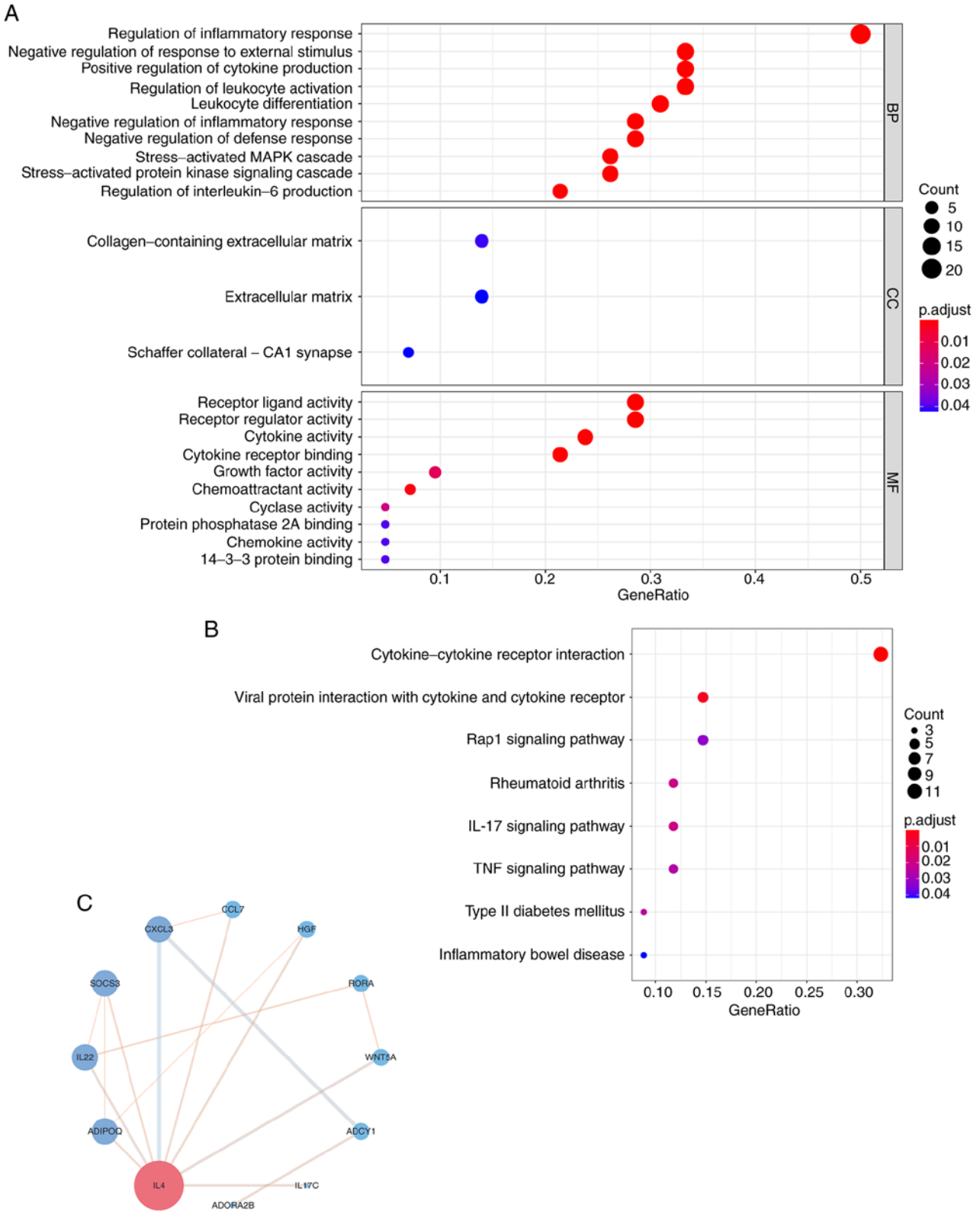

Figure 3. Molecular mechanisms of inflammation-associated genes in the progression of clear cell renal cell carcinoma. (A) Enrichment results of the Gene Ontology annotation, including the top 10 terms in the categories BP, CC and MF. (B) Dysregulated pathways mainly regulated by the inflammation-associated genes. (C) Protein-protein interactive network of the inflammation-associated genes constituting the inflammatory prognostic signature. BP, Biological process; CC, Cellular component; MF, Molecular function.

cohorts. Further correlation analysis found significant positive correlations between the IPS score and the degree of infiltration by M_0 macrophages [ρ=0.18 (training cohort); ρ=0.23 (validation cohort)], CD4 memory-activated T cells [ρ=0.19 (training cohort); ρ=0.12 (validation cohort)], follicular T helper cells [ρ=0.28 (training cohort); ρ=0.28 (validation cohort)] and Tregs [ρ=0.35 (training cohort); ρ=0.32 (validation cohort)]. By contrast, negative correlations were found between the IPS

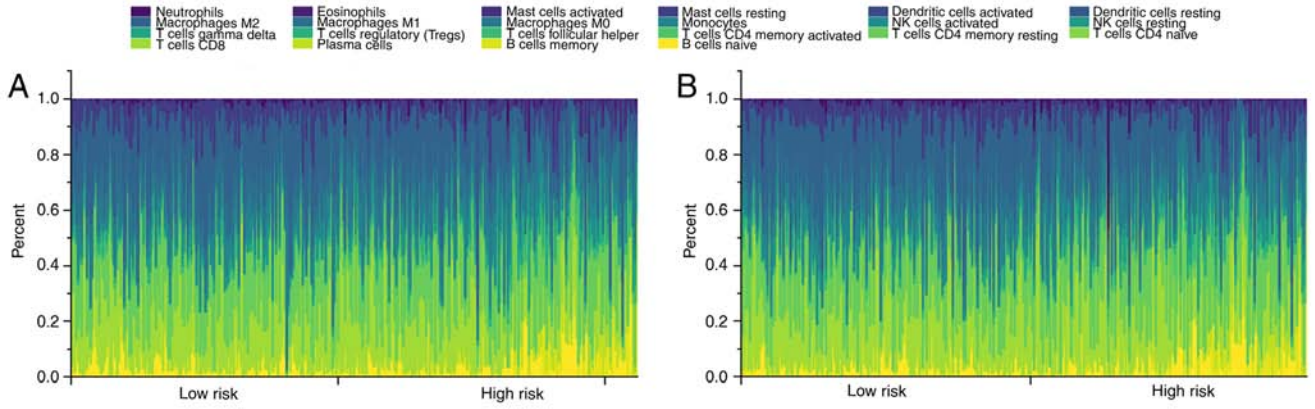

Figure 4. Comprehensive infiltration profiles of immune cells of clear cell renal cell carcinoma. Immune cell profiles in the (A) the training cohort and (B) validation cohort. NK, natural killer.

score and the extent of infiltration by M_2 macrophages [ρ=-0.11 (training cohort); ρ=-0.20 (validation cohort)] and mast cells [ρ=0.24 (training cohort); ρ=-0.29 (validation cohort)]. These identified immune cells were therefore suggested to be important parameters on the prognosis of patients with ccRCC.

Integrated prognostic index (IPI) after combining the IPS with clinicopathological factors. To improve the prediction accuracy of the IPS and to facilitate clinical application, the IPI was constructed using multivariate Cox regression by combining the IPS with the clinicopathological characteristics, namely age, sex and TNM stage. Following feature selection using a stepwise method, the IPI was developed and plotted as a nomogram to calculate the survival probability of individual patients with ccRCC (Fig. 6A). IPI distribution and risk-stratification profiles of the training and validation cohorts are provided in Fig. 6B and C, respectively. Kaplan-Meier curve analysis also revealed that the IPI was able to accurately stratify patients with ccRCC into either low- or high-risk groups, with significantly different survival probabilities (Fig. 6D and E). As expected, the IPI's predictive accuracy in estimating the survival of patients with ccRCC was higher compared with that of the IPS (Fig. 6F), which was observed in both the training [AUC: 0.911 (IPI) vs. 0.811 (IPS)] and validation cohorts [AUC: 0.805 (IPI) vs. 0.799 (IPS)].

Validation in the clinical ccRCC samples. To further validate the IPS developed in the present study, six patients with ccRCC were recruited and their IGP expression was quantified to assign an IPS score using pre-trained IPS model to each subject (Fig. 7). A total of three patients were identified as high-risk whereas the others were low-risk, as determined from the heatmap generated from the qPCR data (Fig. 7C). H&E staining was performed to compare the cell morphology and structure of samples from high-risk and low-risk patients with ccRCC (Fig. 7A). Histologically, samples from high-risk patients with ccRCC identified based on their IPS exhibited more typical malignant findings compared with those of the low-risk cases. In high-risk ccRCC samples, cells had a voluminous, clear and eosinophilic cytoplasm, where their growth patterns were tubular, acinar and lamellar (Fig. 7A). Furthermore, high-risk ccRCC samples also had a papillary or alveolar nested architecture with an abundant vascular network. The tumor cell nuclei exhibited varying degrees of atypia, with features such as prominent nucleoli and spindle-shaped cells. These data suggest that the normal renal tubular epithelium and renal parenchyma were severely damaged in the high-risk ccRCC cells, as compared to their low-risk counterparts, which presented with a moderately damaged renal microstructure. The IHC results further demonstrated that in the high-risk group, the top four risk-associated IGPs were expressed at significantly higher levels compared with those in the low-risk group (Fig. 7B and D), which supported the clinical applicability of the IPS developed in the present study.

Discussion

To the best of our knowledge, the present study was the first to elucidate the prognostic potential of inflammation-associated molecules and develop an IPS for the survival estimation and risk-stratification of patients with ccRCC. The underlying mechanism of the unfavorable prognosis of high-risk patients with ccRCC were identified using the IPS in the present study, where a dysregulated immune microenvironment, signaling pathways and biological functions were revealed. Subsequently, the enhanced prognostic tool IPI combined this IPS with clinicopathological factors, which exhibited greater accuracy for prognosis prediction. With the present study's findings, particularly the IPS and IPI, oncologists may be able pre-stratify patients with ccRCC for optimizing clinical management protocols whilst also improving their understanding into the nature of ccRCC progression in terms of inflammatory responses.

The novelty of the present study lies in the construction of IPS and IPI. Inspired by the key impact of the inflammatory response on the progression of ccRCC (46-48), the prognostic potential of inflammation-associated molecules was systematically elucidated, following which the IPS was developed and validated. This IPS was confirmed to be a viable and robust biomarker for prognostic estimation and risk-stratification in both the training (AUC=0.811) and validation cohorts (AUC=0.799). In addition, IPS was found to be an independent prognostic factor of ccRCC outcomes (P<0.001). The predictive ability of this IPS was higher compared with

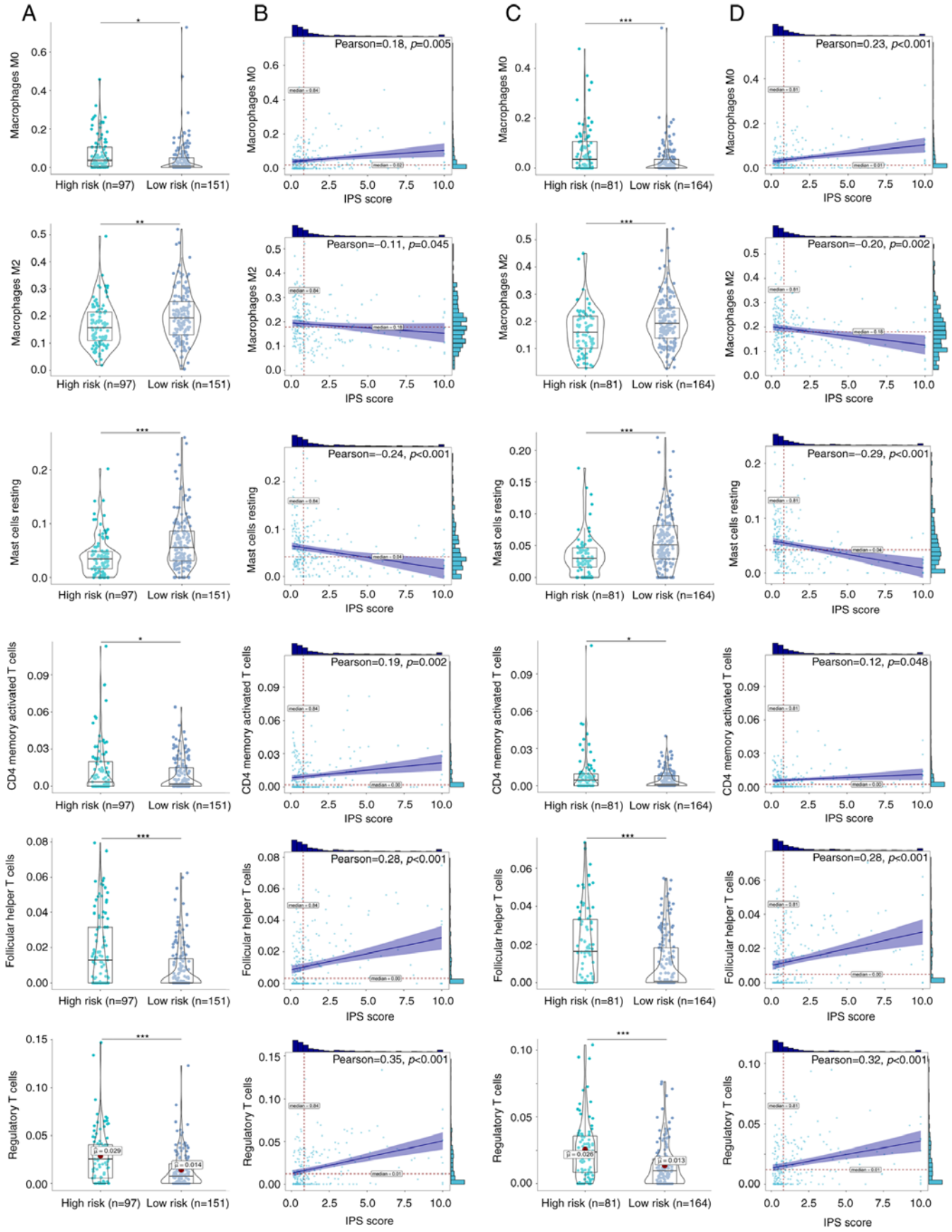

Figure 5. Identified differential infiltrated immune cells in the IPS-identified high- and low-risk ccRCC groups. (A) Infiltration of six types of immune cells compared between the IPS-identified high- and low-risk ccRCC groups in the training cohort. (B) Correlations between those immune cell types and the IPS score in the training cohort. A violin plot is a hybrid of a box plot and a kernel density plot, which shows peaks in the data, and dots indicate each data point. Bars above and to the right of the plot represent frequency of the corresponding values. (C) Infiltration of six types of immune cells compared between the IPS-identified high- and low-risk ccRCC groups in the validation cohort. (D) Correlations between those immune cells and the IPS score in the validation cohort. ccRCC, clear cell renal cell carcinoma; IPS, inflammatory prognostic signature. *P<0.05, **P<0.01 and ***P<0.001.

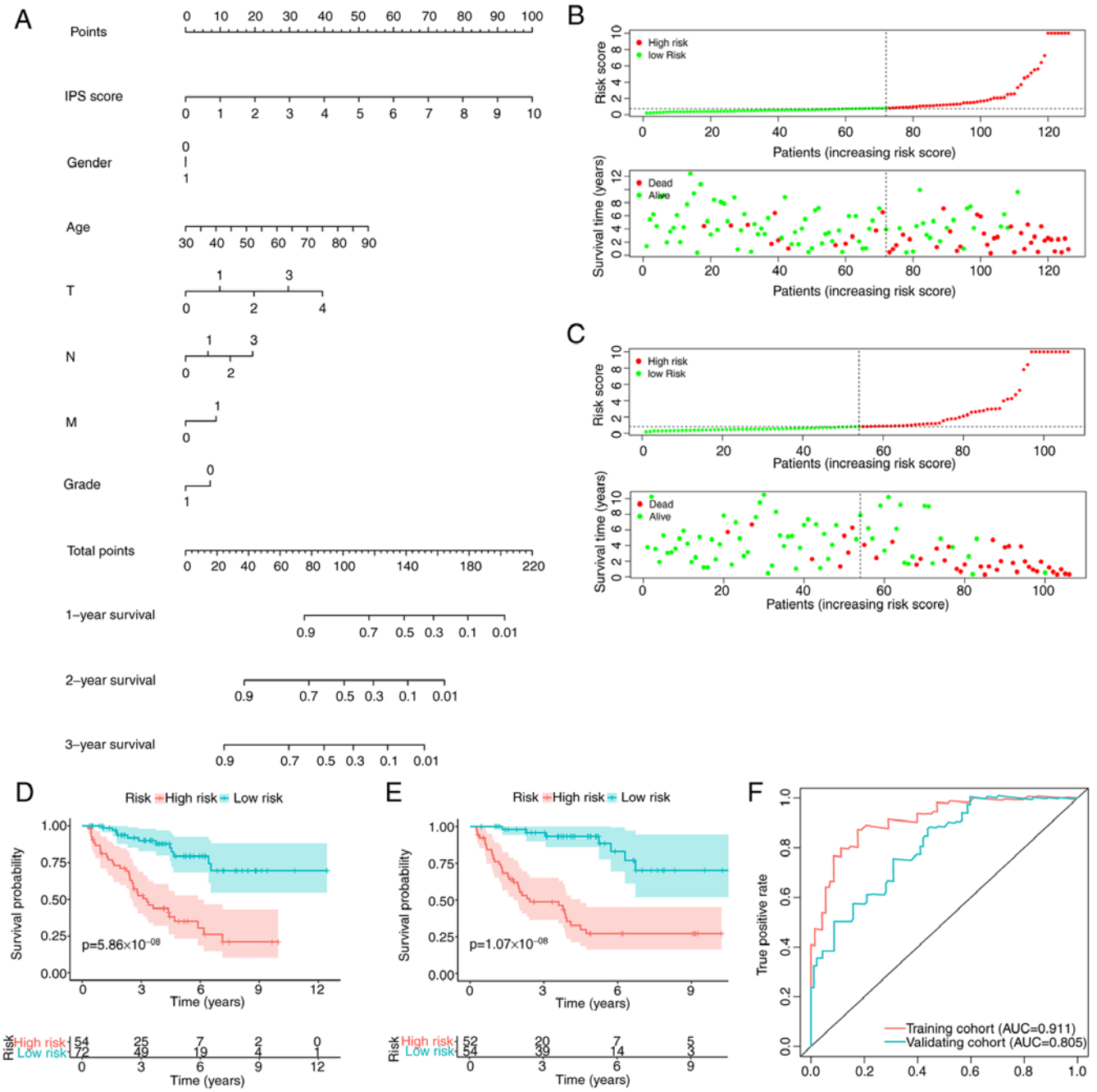

Figure 6. Construction and validation of an IPI. (A) Nomogram of the IPI. IPS score, overall survival time and survival status of each patient with ccRCC in (B) the training and (C) validation cohorts. Kaplan-Meier curves indicating the difference in survival probability between patients with ccRCC in the high- and low-risk groups from the (D) training and (E) validation cohorts. (F) ROC curve of the IPI. IPS, inflammatory prognostic signature; IPI, integrated prognostic index; ccRCC, clear cell renal cell carcinoma; AUC, area under the ROC curve; ROC, receiver operating characteristic.

that of the other reported biomarkers (immune-related risk signature with AUC of 0.753) (24,49), suggesting that inflammation-associated molecules are of high prognostic value for ccRCC. This IPS was also discovered to be a high-risk factor for poorer outcomes compared with other clinical characteristics [HR=11.73; 95% CI, 26.98-5.10; P<0.001], yielding the largest HR in the present study. Subsequently, the IPI was developed by combining the IPS with clinicopathological factors to enhance clinical accuracy. In the nomogram of the IPI, the score for each feature was calculated to obtain the total score, before a vertical line is drawn on the total score scale to enable clinicians to estimate the expected survival probability of an individual patient with ccRCC. IPI displayed higher accuracy compared with IPS for prognostic estimation in both the training [AUC: 0.911 (IPI) vs. 0.811 (IPS)] and validation cohorts [AUC: 0.805 (IPI) vs. 0.799 (IPS)]. Using this proposed tool, in-clinic risk-stratification of ccRCC could be improved in terms of both accuracy and convenience. In addition, as tumorigenesis and development of solid carcinomas in humans are facilitated by a strong proinflammatory environment (50-52), it is hypothesized that the IPS score, which was constructed using IGs, can perform well when applied for the prognosis estimation of other tumor types, such as neuroblastoma or osteosarcoma.

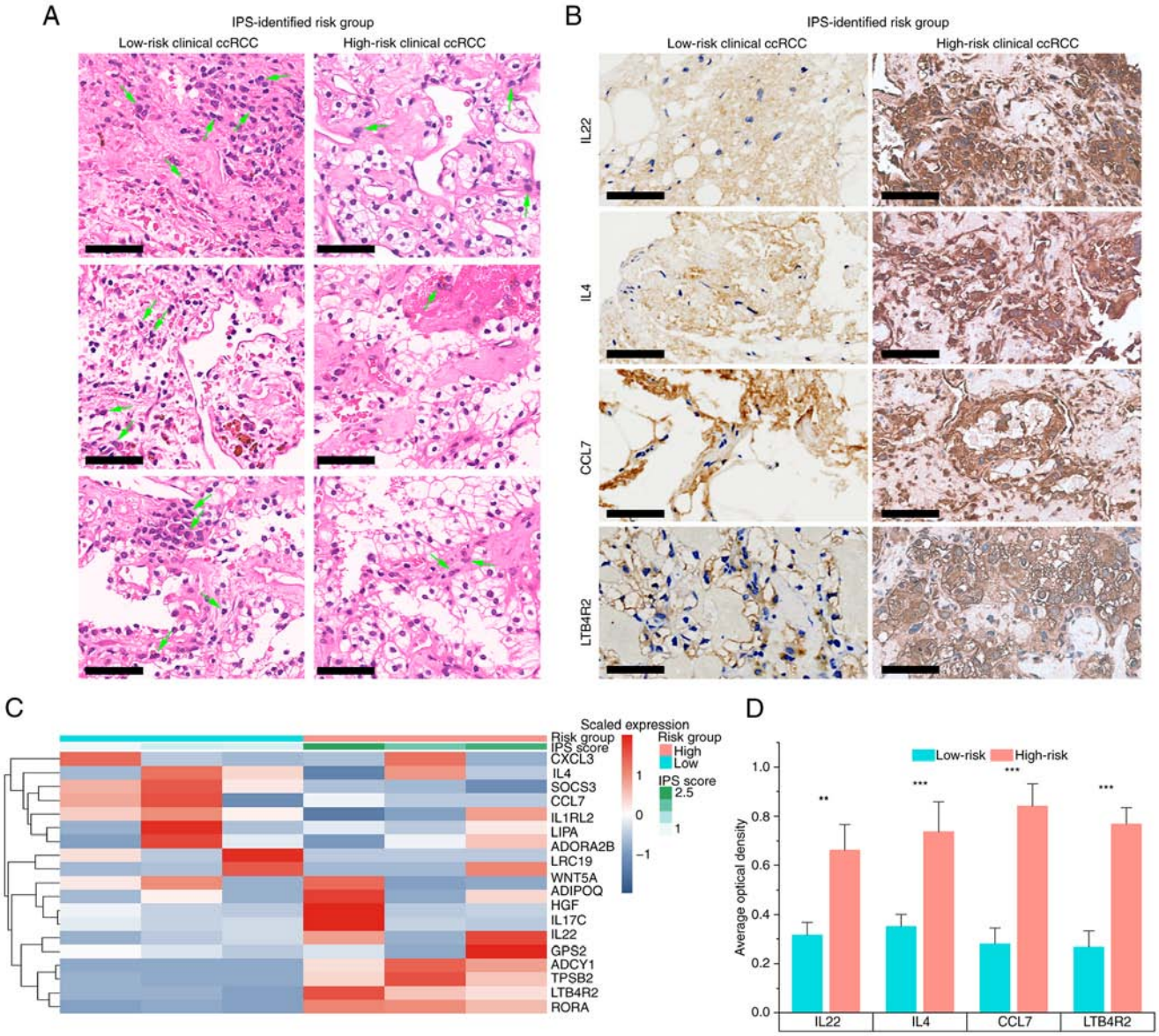

Figure 7. Clinical validation of the IPS. (A) H&E staining results of IPS-identified high- and low-risk ccRCC samples. Arrows indicate some macrophage examples. (B) IHC results of the top four most hazardous IGPs. All scale bars are 50 μm. (C) IGP expression and IPS score of each patient with ccRCC. (D) Quantification of IHC results of the top four most hazardous IGPs. ccRCC, clear cell renal cell carcinoma; IPS, inflammatory prognostic signature. CCL7, C-C motif chemokine ligand 7; LTB4R2, leukotriene B4 receptor 2. **P<0.01 and ***P<0.001.

The immune microenvironment serves a significant role in tumor development (17), particularly in ccRCC (53-55). Numerous studies have previously revealed that the interaction between inflammation and immune cells can potentially fuel the malignant development of ccRCC (44,45). In particular, inflammatory signaling pathways [e.g., von Hippel-Lindau tumor suppressor (VHL), hypoxia, TNF-α, STAT and TGF-β] and inflammatory molecules (e.g., pVHL, TGFβ, IL6 and selected chemokines/chemokine receptors) can promote the tumor evasion of immune cells (44). As a type of inflammatory cell death, pyroptosis may also recast a suitable immune microenvironment to promote ccRCC growth (45). However, only a small number of studies have systematically investigated the association between an RNA expression-based inflammatory signature and the immune microenvironment in the development of ccRCC (56). In the present study, high-risk ccRCCs were classified based on the IPS, which exhibited dysregulated profiles of immune cell infiltration compared with those of low-risk ccRCCs. Infiltration by M_0 macrophages, CD4 memory activated T cells, follicular helper T cells and Tregs were all found to be significantly increased in high-risk ccRCC. These tumor-infiltrating immune cells present at high levels are proposed to sculpt a highly immunosuppressive microenvironment to potentially promote the development of tumors, particularly ccRCC (49,57). In a previous study, M_0 macrophages were found to facilitate the progression of ccRCC, where they were present at high levels in high-risk patients with ccRCC (49). Tregs normally prevent hyperactive immune responses and autoimmunity (58). They have been reported to accumulate aberrantly in tumors, where they suppress antitumor immunity and support the establishment of an immunosuppressive microenvironment (58). All these aforementioned results strongly indicate that the dysregulation of immune cells or the immune microenvironment can fuel the

progression of high-risk ccRCC, which was identified by the IPS in the present study.

There are certain limitations to the present study. Although analysis was performed using a large sample size, the retrospective nature is a limitation. Therefore, these findings, including IPS and IPI, require further validation in clinical trials. Furthermore, the IPS and associated immune mechanisms require further validation using clinical data from multiple centers. It was also not possible to analyze disease-free survival due to the high abundance of censored data. Experimental *in vitro* and *in vivo* data are expected to strengthen the clinical feasibility of the IPS, which will be pursued further as planned for future studies.

In conclusion, data in the present study suggest that the constructed IPS and IPI are a highly effective and robust tools for the clinical pre-stratification of patients with ccRCC for the precise designation of intervention strategies to enhance survival probability. Subsequently, it was found that inflammatory responses and the dysregulation of the immune microenvironment, including higher infiltration of immunosuppressive cells, can fuel the progression of ccRCC. It is hoped that these findings can facilitate the biological understanding into the roles of immunity and inflammation in ccRCC development.

Acknowledgements

Not applicable.

Funding

The present study was supported by a grant for the Hainan Provincial Natural Science Foundation of China (grant no. 820RC769 and grant no.822RC839) and Hainan Provincial Graduate Innovation research project (grant no. Qhyb2021-57).

Availability of data and materials

The datasets used and/or analyzed during the current study are available from the corresponding author on reasonable request.

Authors' contributions

GL was responsible for conceptualization and visualization. GL and DX helped with the methodology, data curation and writing (original draft preparation). GL, DX and ZC performed the formal analysis. WJ, ZC and HC were involved in writing (reviewing and editing for important intellectual content), and helped with the analysis. WJ and ZC controlled project administration. HC was responsible for funding acquisition. ZC and HC confirm the authenticity of all the raw data. All authors read and approved the final manuscript.

Ethics approval and consent to participate

Full informed consent in written form was given by the subjects and the study was approved by the Ethics Committee of Renmin Hospital of Wuhan University (Wuhan, China; approval no. 2017K-C015).

Patient consent for publication

Not applicable.

Competing interests

The authors declare that they have no competing interests.

References

1. Che Z, Fan J, Zhou Z, Li Q, Ma Z, Hu Z, Wu Y, Jin Y, Su Y, Liang P and Li H: Activation-induced cytidine deaminase expression facilitates the malignant phenotype and epithelial-to-mesenchymal transition in clear cell renal cell carcinoma. DNA Cell Biol 39: 1299-1312, 2020.
2. Zhang F, Ma X, Li H, Zhang Y, Li X, Chen L, Guo G, Gao Y, Gu L, Xie Y, *et al*: FOXK2 suppresses the malignant phenotype and induces apoptosis through inhibition of EGFR in clear-cell renal cell carcinoma. Int J Cancer 142: 2543-2557, 2018.
3. Wang Y, Cong R, Liu S, Zhu B, Wang X and Xing Q: Decreased expression of METTL14 predicts poor prognosis and construction of a prognostic signature for clear cell renal cell carcinoma. Cancer Cell Int 21: 46, 2021.
4. Tacconi EM, Tuthill M and Protheroe A: Review of adjuvant therapies in renal cell carcinoma: Evidence to date. Onco Targets Ther 13: 12301-12316, 2020.
5. Su Y, Lu J, Chen X, Liang C, Luo P, Qin C and Zhang J: Long non-coding RNA HOTTIP affects renal cell carcinoma progression by regulating autophagy via the PI3K/Akt/Atg13 signaling pathway. J Cancer Res Clin Oncol 145: 573-588, 2019.
6. Xu F, Guan Y, Xue L, Huang S, Gao K, Yang Z and Chong T: The effect of a novel glycolysis-related gene signature on progression, prognosis and immune microenvironment of renal cell carcinoma. BMC Cancer 20: 1207, 2020.
7. Czarnecka AM, Kukwa W, Kornakiewicz A, Lian F and Szczylik C: Clinical and molecular prognostic and predictive biomarkers in clear cell renal cell cancer. Future Oncol 10: 2493-2508, 2014.
8. Wang ZH, Zhang YZ, Wang YS and Ma XX: Identification of novel cell glycolysis related gene signature predicting survival in patients with endometrial cancer. Cancer Cell Int 19: 296, 2019.
9. Gray RE and Harris GT: Renal cell carcinoma: Diagnosis and management. Am Fam Physician 99: 179-184, 2019.
10. Shi J, Wang K, Xiong Z, Yuan C, Wang C, Cao Q, Yu H, Meng X, Xie K, Cheng Z, *et al*: Impact of inflammation and immunotherapy in renal cell carcinoma. Oncol Lett 20: 272, 2020.
11. Zhao E, Li L, Zhang W, Wang W, Chan Y, You B and Li X: Comprehensive characterization of immune- and inflammation-associated biomarkers based on multi-omics integration in kidney renal clear cell carcinoma. J Transl Med 17: 177, 2019.
12. Chen Q, Wang J, Zhang Q, Zhang J, Lou Y, Yang J, Chen Y, Wei T, Zhang J, Fu Q, *et al*: Tumour cell-derived debris and IgG synergistically promote metastasis of pancreatic cancer by inducing inflammation via tumour-associated macrophages. Br J Cancer 121: 786-795, 2019.
13. Balkwill F and Mantovani A: Inflammation and cancer: Back to Virchow? Lancet 357: 539-545, 2001.
14. Liubomirski Y, Lerrer S, Meshel T, Rubinstein-Achiasaf L, Morein D, Wiemann S, Körner C and Ben-Baruch A: Tumor-stroma-inflammation networks promote pro-metastatic chemokines and aggressiveness characteristics in triple-negative breast cancer. Front Immunol 10: 757, 2019.
15. Ngabire D and Kim GD: Autophagy and inflammatory response in the tumor microenvironment. Int J Mol Sci 18: 2016, 2017.
16. Carraway RE and Cochrane DE: Enhanced vascular permeability is hypothesized to promote inflammation-induced carcinogenesis and tumor development via extravasation of large molecular proteins into the tissue. Med Hypotheses 78: 738-743, 2012.
17. Mantovani A, Bussolino F and Dejana E: Cytokine regulation of endothelial cell function. FASEB J 6: 2591-2599, 1992.
18. Dominguez C, David JM and Palena C: Epithelial-mesenchymal transition and inflammation at the site of the primary tumor. Semin Cancer Biol 47: 177-184, 2017.
19. Koong AC, Denko NC, Hudson KM, Schindler C, Swiersz L, Koch C, Evans S, Ibrahim H, Le QT, Terris DJ and Giaccia AJ: Candidate genes for the hypoxic tumor phenotype. Cancer Res 60: 883-887, 2000.

20. Taher MY, Davies DM and Maher J: The role of the interleukin (IL)-6/IL-6 receptor axis in cancer. Biochem Soc Trans 46: 1449-1462, 2018.
21. Kaminska K, Czarnecka AM, Escudier B, Lian F and Szczylik C: Interleukin-6 as an emerging regulator of renal cell cancer. Urol Oncol 33: 476-485, 2015.
22. DiGiacomo JW and Gilkes DM: Tumor hypoxia as an enhancer of inflammation-mediated metastasis: Emerging therapeutic strategies. Target Oncol 13: 157-173, 2018.
23. Simon N, Friedman J, Hastie T and Tibshirani R: Regularization paths for Cox's proportional hazards model via coordinate descent. J Stat Softw 39: 1-13, 2011.
24. Jin W, Zhang Y, Liu Z, Che Z, Gao M and Peng H: Exploration of the molecular characteristics of the tumor-immune interaction and the development of an individualized immune prognostic signature for neuroblastoma. J Cell Physiol 236: 294-308, 2021.
25. Therneau TM and Grambsch PM: Modeling survival data: Extending the Cox model. Springer, New York, NY, pp39-77, 2000.
26. Li B, Cui Y, Diehn M and Li R: Development and validation of an individualized immune prognostic signature in early-stage nonsquamous non-small cell lung cancer. JAMA Oncol 3: 1529-1537, 2017.
27. Newman AM, Liu CL, Green MR, Gentles AJ, Feng W, Xu Y, Hoang CD, Diehn M and Alizadeh AA: Robust enumeration of cell subsets from tissue expression profiles. Nat Methods 12: 453-457, 2015.
28. Liu L, Huang L, Chen W, Zhang G, Li Y, Wu Y, Xiong J and Jie Z: Comprehensive analysis of necroptosis-related long noncoding RNA immune infiltration and prediction of prognosis in patients with colon cancer. Front Mol Biosci 9: 811269, 2022.
29. Livak KJ and Schmittgen TD: Analysis of relative gene expression data using real-time quantitative PCR and the 2(-Delta Delta C(T)) method. Methods 25: 402-408, 2001.
30. Xiao Z, He L, Takemoto M, Jalanko H, Chan GC, Storm DR, Betsholtz C, Tryggvason K and Patrakka J: Glomerular podocytes express type 1 adenylate cyclase: Inactivation results in susceptibility to proteinuria. Nephron Exp Nephrol 118: e39-e48, 2011.
31. Saleh AA, Tayel SI, Shalaby AG and El Naidany SS: Role of adiponectin gene and receptor polymorphisms and their mRNA levels with serum adiponectin level in myocardial infarction. Appl Clin Genet 13: 241-252, 2020.
32. Mertens TC, Hanmandlu A, Tu L, Phan C, Collum SD, Chen NY, Weng T, Davies J, Liu C, Eltzschig HK, *et al*: Switching-Off Adora2b in vascular smooth muscle cells halts the development of pulmonary hypertension. Front Physiol 9: 555, 2018.
33. Feuser K, Thon KP, Bischoff SC and Lorentz A: Human intestinal mast cells are a potent source of multiple chemokines. Cytokine 58: 178-185, 2012.
34. Berglöf E, Andre R, Renshaw BR, Allan SM, Lawrence CB, Rothwell NJ and Pinteaux E: IL-1Rrp2 expression and IL-1F9 (IL-1H1) actions in brain cells. J Neuroimmunol 139: 36-43, 2003.
35. Chai L, Dai L, Che Y, Xu J, Liu G, Zhang Z and Yang R: LRRC19, a novel member of the leucine-rich repeat protein family, activates NF-kappaB and induces expression of proinflammatory cytokines. Biochem Biophys Res Commun 388: 543-548, 2009.
36. Venerito M, Helmke C, Jechorek D, Wex T, Rosania R, Antweiler K, Weigt J and Malfertheiner P: Leukotriene receptor expression in esophageal squamous cell cancer and non-transformed esophageal epithelium: A matched case control study. BMC Gastroenterol 16: 85, 2016.
37. Liu B, Xie Y, Mei X, Sun Y, Shi W and Wu Z: Reciprocal regulation of interleukin-17A and interleukin-22 secretion through aryl hydrocarbon receptor activation in CD4(+) T cells of patients with vitiligo. Exp Ther Med 21: 158, 2021.
38. Cai X, Zhang P, Wang S, Hong L, Yu S, Li B, Zeng H, Yang X and Shao L: lncRNA FGD5 antisense RNA 1 upregulates RORA to suppress hypoxic injury of human cardiomyocyte cells by inhibiting oxidative stress and apoptosis via miR195. Mol Med Rep 22: 4579-4588, 2020.
39. Flores-Mendoza LK, Estrada-Jimenez T, Sedeno-Monge V, Moreno M, Manjarrez MD, González-Ochoa G, Millán-Pérez Peña L and Reyes-Leyva J: IL-10 and socs3 are predictive biomarkers of dengue hemorrhagic fever. Mediators Inflamm 2017: 5197592, 2017.
40. Liang Y, Qiao L, Peng X, Cui Z, Yin Y, Liao H, Jiang M and Li L: The chemokine receptor CCR1 is identified in mast cell-derived exosomes. Am J Transl Res 10: 352-367, 2018.
41. Wu J, Lv Y, Li Y, Jiang Y, Wang L, Zhang X, Sun M, Zou Y, Xu J and Zhang L: MCM3AP-AS1/miR-876-5p/WNT5A axis regulates the proliferation of prostate cancer cells. Cancer Cell Int 20: 307, 2020.
42. Patil I: Visualizations with statistical details: The'ggstatsplot' approach. J Open Source Softw 6: 3167, 2021.
43. Alba AC, Agoritsas T, Walsh M, Hanna S, Iorio A, Devereaux PJ, McGinn T and Guyatt G: Discrimination and calibration of clinical prediction models: Users' guides to the medical literature. JAMA 318: 1377-1384, 2017.
44. de Vivar Chevez AR, Finke J and Bukowski R: The role of inflammation in kidney cancer. Adv Exp Med Biol 816: 197-234, 2014.
45. Zhang X, Wei X, Wang Y, Wang S, Ji C, Yao L and Song N: Pyroptosis regulators and tumor microenvironment infiltration characterization in clear cell renal cell carcinoma. Front Oncol 11: 774279, 2021.
46. Nishida J, Momoi Y, Miyakuni K, Tamura Y, Takahashi K, Koinuma D, Miyazono K and Ehata S: Epigenetic remodelling shapes inflammatory renal cancer and neutrophil-dependent metastasis. Nat Cell Biol 22: 465-475, 2020.
47. Gorka J, Marona P, Kwapisz O, Rys J, Jura J and Miekus K: The anti-inflammatory protein MCPIP1 inhibits the development of ccRCC by maintaining high levels of tumour suppressors. Eur J Pharmacol 888: 173591, 2020.
48. Roumenina LT, Daugan MV, Noé R, Petitprez F, Vano YA, Sanchez-Salas R, Becht E, Meilleroux J, Clec'h BL, Giraldo NA, *et al*: Tumor cells hijack macrophage-produced complement C1q to promote tumor growth. Cancer Immunol Res 7: 1091-1105, 2019.
49. Hua X, Chen J, Su Y and Liang C: Identification of an immune-related risk signature for predicting prognosis in clear cell renal cell carcinoma. Aging (Albany NY) 12: 2302-2332, 2020.
50. Vezzani B, Carinci M, Previati M, Giacovazzi S, Della Sala M, Gafà R, Lanza G, Wieckowski MR, Pinton P and Giorgi C: Epigenetic regulation: A link between inflammation and carcinogenesis. Cancers (Basel) 14: 1221, 2022.
51. Özdemir BH: Tumor microenvironment: Necroptosis switches the subtype of liver cancer while necrosis promotes tumor recurrence and progression. Exp Clin Transplant: Mar 15, 2022 (Epub ahead of print).
52. Jha NK, Arfin S, Jha SK, Kar R, Dey A, Gundamaraju R, Ashraf GM, Gupta PK, Dhanasekaran S, Abomughaid MM, *et al*: Re-establishing the comprehension of phytomedicine and nanomedicine in inflammation-mediated cancer signaling. Semin Cancer Biol: Feb 23, 2022 (Epub ahead of print).
53. Şenbabaoğlu Y, Gejman RS, Winer AG, Liu M, Van Allen EM, de Velasco G, Miao D, Ostrovnaya I, Drill E, Luna A, *et al*: Tumor immune microenvironment characterization in clear cell renal cell carcinoma identifies prognostic and immunotherapeutically relevant messenger RNA signatures. Genome Biol 17: 231, 2016.
54. Chevrier S, Levine JH, Zanotelli VR, Silina K, Schulz D, Bacac M, Ries CH, Ailles L, Jewett MA, Moch H, *et al*: An immune atlas of clear cell renal cell carcinoma. Cell 169: 736-749.e718, 2017.
55. Xiao GF, Yan X, Chen Z, Zhang RJ, Liu TZ and Hu WL: Identification of a novel immune-related prognostic biomarker and small-molecule drugs in clear cell renal cell carcinoma (ccRCC) by a merged microarray-acquired dataset and TCGA database. Front Genet 11: 810, 2020.
56. Tang X, Zhang A, Feng Y, Su Y, Wang X, Jiang F and Ma J: A novel pyroptosis-related lncRNAs signature for predicting the prognosis of kidney renal clear cell carcinoma and its associations with immunity. J Oncol 2021: 9997185, 2021.
57. Dunn GP, Bruce AT, Ikeda H, Old LJ and Schreiber RD: Cancer immunoediting: From immunosurveillance to tumor escape. Nat Immunol 3: 991-998, 2002.
58. Wang H, Franco F and Ho PC: Metabolic regulation of tregs in cancer: Opportunities for immunotherapy. Trends Cancer 3: 583-592, 2017.

This work is licensed under a Creative Commons Attribution-NonCommercial-NoDerivatives 4.0 International (CC BY-NC-ND 4.0) License.